Published in final edited form as:

Ultrasound Med Biol. 2015 July ; 41(7): 1896–1904. doi:10.1016/j.ultrasmedbio.2015.02.012.

Quantification of microvascular tortuosity during tumor evolution utilizing acoustic angiography

Sarah E. Shelton[1], **Yueh Z. Lee**[2,5], **Mike Lee**[3], **Emmanuel Cherin**[3], **F. Stuart Foster**[3], **Stephen R. Aylward**[4], and **Paul A. Dayton**[1,5]

[1] Joint Department of Biomedical Engineering, University of North Carolina at Chapel Hill and North Carolina State University, CB7575, Chapel Hill, NC 27599

[2] Department of Neuroradiology, University of North Carolina at Chapel Hill, CB#7510, Chapel Hill, NC 27599

[3] Department of Medical Biophysics, Sunnybrook Health Sciences Centre, Toronto, ON, Canada

[4] Kitware Medical Imaging, 101 East Weaver Street, Carrboro, NC

[5] Biomedical Research Imaging Center, University of North Carolina at Chapel Hill, Marsico Hall, Chapel Hill, NC 27599

Abstract

The recent design of ultra-broadband, multi-frequency ultrasound transducers has enabled high sensitivity, high-resolution contrast imaging, with very efficient suppression of tissue background using a technique called acoustic angiography. Here we perform the first application of acoustic angiography to evolving tumors in mice predisposed to develop mammary carcinoma, with the intent of visualizing and quantifying angiogenesis progression associated with tumor growth. Metrics compared include vascular density and two measures of vessel tortuosity quantified from segmentations of vessels traversing and surrounding 24 tumors and abdominal vessels from control mice. Quantitative morphological analysis of tumor vessels demonstrated significantly increased vascular tortuosity abnormalities associated with tumor growth with the distance metric elevated approximately 14% and the sum of angles metric increased 60% in tumor vessels versus controls. Future applications of this imaging approach may provide clinicians a new tool in tumor detection, differentiation, or evaluation, though with limited depth of penetration using the current configuration.

Keywords

tortuosity; contrast agent; microbubble; ultrasound; acoustic angiography; microvasculature; angiogenesis; superharmonic imaging

Corresponding author: Paul Dayton, Ph.D., UNC-NCSU Joint Department of Biomedical Engineering, 152 MacNider Hall, CB7575, Chapel Hill, NC, 27599, phone: (919) 843 9521, fax: (919) 843 9520, padayton@email.unc.edu.

Introduction

Ultrasound imaging has several advantages over other modalities in the clinic such as low cost, portability, safety, and real-time imaging capability. However, grayscale ultrasound suffers from speckle noise and has poor sensitivity to blood flow in small vessels. Contrast-enhanced ultrasound (CEUS) utilizes administration of a microbubble contrast agent to enhance imaging sensitivity to blood flow, and is primarily utilized for enhanced delineation of the left ventricle in echocardiography. Quantitative CEUS imaging, including techniques such as wash-in and wash-out curves have been widely utilized in oncology imaging because of the involvement of vascular networks in tumor progression (Quaia 2011). Current CEUS imaging is performed at clinically-relevant frequencies between 1-12 MHz, and utilizes techniques such as pulse-inversion and amplitude-modulation in order to enhance detection of microbubbles and reduce tissue background (Averkiou et al. 2003; Martin and Dayton 2013). However, these strategies also limit both the resolution and contrast-to-tissue ratio of existing CEUS imaging.

Acoustic angiography is a significant advance in contrast-enhanced ultrasound (CEUS) imaging made possible by the application of dual-frequency ultrasound transducers, which as of yet are still only available as prototype devices (Gessner et al. 2013). In acoustic angiography imaging, microbubble contrast agents are excited by a low frequency ultrasound transducer element, similar to those used in clinical imaging (2-4 MHz), yet imaging data is received with a second transducer at a much higher frequency, e.g. 25-30 MHz using the technology described here. The excited microbubbles produce broadband superharmonic energy, which can be detected with the high frequency receiver, whereas tissue scatters almost negligible energy at this frequency (Kruse and Ferrara 2005). This dual-frequency approach results in images of the contrast agent only (flowing through the microvessels) with very minimal if any tissue background. The resulting images obtained with this new technique demonstrate images of blood vessel morphology entirely unlike standard B-mode ultrasound and resembling x-ray angiograms, thus leading us to refer to this technique as "acoustic angiography". An additional substantial advantage is that the dual-frequency approach enables resolution as dictated by the high frequency receiver, although this also provides a limitation in penetration depth due to (one-way) attenuation of high frequency signals from the microbubbles (Lindsey et al. 2014). Figure 1 depicts a side-by-side comparison of B-mode and acoustic angiography (maximum intensity projection) images of the same tissue volume, approximately 2.5 by 2.5 cm, in the coronal view, illustrating the advantages of acoustic angiography in assessing microvascular structure.

Because acoustic angiography can image microvessel structure, it is an ideal tool for visualizing abnormal vascular morphology resulting from cancer angiogenesis. Angiogenesis is the process of new vascular growth, which is a necessary process for physiologic events such as wound healing (Nissen et al. 1998), but escapes normal pathologic control during tumor development. Malignant angiogenesis is so pervasive across different types of tumors that it is one of Hanahan and Weinberg’s “Hallmarks of Cancer” (Hanahan and Weinberg 2011). Judah Folkman was one of the first researchers to realize the importance of angiogenesis in cancer and posited that tumors would not grow beyond 2-3 mm in size without neovascularization (Folkman 1971), and the present work will show that

2-3 mm tumors do indeed show quantifiable angiogenesis in the mouse model chosen. A number of mechanisms of tumor angiogenesis exist, driven by different pro-angiogenic growth factors and molecular pathways (Carmeliet and Jain 2011). However, the end result of such abundant pro-angiogenic processes is a vascular network that is abnormal in both form and function. Tumor vessel networks lack the ordered, hierarchical branching networks found in normal tissue; vessels are leaky, tortuous, and have unpredictable relationships between size and flow rate (Jain et al. 2014). The angiogenic factors produced by tumors (such as vascular endothelial growth factor, or VEGF) often cause increased vessel diameter, vascular density, permeability, as well as alterations in vessel structure (Jain 2005; Jain 2014). Acoustic angiography has the unique potential to improve visualization and quantification of some of these angiogenic changes.

The microvascular maps produced by acoustic angiography have sufficient contrast and detail that computerized segmentation using multi-scale ridge traversal for centerline extraction (Aylward and Bullitt 2002) can be used to define the spatial coordinates occupied by individual vessels. From the spatial coordinates, the “curvedness”, or tortuosity, of the vessels can be computed, enabling the definition of multiple descriptions of vessel shape. It is the quantification of these tortuosity metrics which provides a new way to describe tumors using ultrasound imaging (Gessner et al. 2012). Tortuosity associated with malignancy has been used previously with other imaging modalities such as magnetic resonance angiography (MRA), photoacoustic tomography, microscopy, and computed tomography (CT) (Jain 2003; Bullitt et al. 2004; Bullitt et al. 2005b; Bullitt et al. 2006; Badea et al. 2008; Laufer et al. 2012; Sodi et al. 2013). However, ultrasound applications of tortuosity metrics have primarily been limited to quantification of skeletonizations from intensity thresholding of Doppler ultrasound images (Huang et al. 2008; Molinari et al. 2010; Chang et al. 2012; Molinari et al. 2014). These types of images lack the clear vessel structures visible in acoustic angiography which make segmentation and analysis of tortuosity in individual vessels possible.

This study uses animal models to study vascular reformation associated with basal breast cancer. Basal breast cancer was chosen because it represents a significant disease burden and current diagnostic imaging suffers from poor specificity. Additionally, the breast provides an attractive target for the clinical translation of acoustic angiography imaging of lesions within a few centimeters of the skin surface (Feig et al. 1977). The vascular images produced by acoustic angiography offer the potential to identify malignant lesions through the quantification of the fundamental biologic process of cancer angiogenesis, and to become a useful clinical tool for evaluating suspicious lesions and for monitoring patients with known pathologies. The focus of the following studies is to demonstrate that tortuosity measures are higher than control levels in the smallest tumors palpable in mouse mammary pads (2-3 mm), and to explore how these metrics are related to tumor size.

Materials and Methods

Animal studies were approved by the University of North Carolina Institutional Animal Care and Use Committee. The UNC Lineberger Comprehensive Cancer Center's Mouse Phase I Unit (MP1U) provided C3(1)/Tag mice that are genetically engineered models of

basal breast cancer. Tumors are formed spontaneously in the mammary pad due to inactivation of the p53 and Rb (retinoblastoma) genes by the Simian Virus 40 large T antigen (Duncan et al. 2012). Control mice were female littermates not carrying the tumor suppressor gene inactivation to provide age, sex, and species matched controls.

Imaging was performed after anesthetizing the mice with vaporized isoflurane and placing them on a heated stage in the supine position. The abdomen was shaved and depilated, and ultrasound gel was applied to couple the transducer to the skin. Ultrasound images were acquired on a Vevo 770 ultrasound scanner (VisualSonics, Toronto, CA) with modified RMV 707 (30 MHz) or RMV 710B (25 MHz) transducers with 4 MHz annular transducers added for microbubble excitation in dual-frequency mode (Gessner et al. 2010). B-mode images of the inguinal mammary pads were acquired with the high frequency transducer, and the B-mode images were used to measure the dimensions of each tumor. The maximum imaging depth of all images acquired was 2.5 cm, which was more than adequate for visualization of mouse mammary pads and all tumors. Frame rate (4.5 frames per second) and inter-frame step size (100 microns) was kept consistent for all images acquired in this study.

Dual-frequency mode was used to acquire acoustic angiography images immediately following the acquisition of B-mode images, exciting the low frequency element with a single-cycle, inverted sinusoidal pulse to produce a transmit pulse with a mechanical index (MI) of approximately 0.6, and using the high frequency element to receive only.

Lipid-encapsulated microbubble contrast agents containing decafluorobutane (SynQuest Labs, Alachua, FL) were prepared with a (9:1) molar mixture of 1,2-distearoyl-sn-glycero-3-phosphocholine (DSPC, Avanti Polar Lipids, Alabaster, AL), and 1,2-distearoyl-sn -glycero-3-phosphoethanolamine-N-[methoxy(polyethylene glycol)-2000] (mPEG-DSPE, Creative PEGWorks, Winston Salem, NC) and phosphate-buffered saline in phosphate-buffered saline containing 15% (v/v) propylene glycol and 5% (v/v) glycerol, as described previously (Feingold et al. 2010). The lipid solution was agitated with a Vialmix mixer (Bristol-Myers Squibb Medical Imaging, North Billerica, MA) to create microbubbles which were infused through a tail-vein catheter at a rate of 1.5×10^8 bubbles/minute during acoustic angiography imaging.

Two acoustic angiography frames were acquired at each location and averaged to provide modest image smoothing. The 100 micron elevational steps used to acquire a 3-D volume were linearly interpolated to form isotropic, 50 micron voxels using Matlab (The MathWorks Inc., Natick, MA). Individual vessels were segmented using the Aylward/Bullitt centerline extraction algorithm with manually-defined seed points (Aylward and Bullitt 2002). Statistical analysis was performed in R (R Foundation for Statistical Computing, Vienna, Austria)(R Development Core Team 2012).

Vascular tortuosity within and surrounding a tumor can be defined in a number of ways for three-dimensional objects. For the analysis described here, we used two metrics to capture different types of tortuosity seen in abnormal angiogenesis, and described in detail by Bullitt et al. (Bullitt et al. 2003) First, the distance metric (DM) is calculated as the total path length

of a vessel, divided by the Euclidean distance between vessel endpoints. The DM has a minimum value of 1 for a vessel lying in a straight line and increases as the vessel deviates from straight. The DM is effective at measuring arching curves, but is less sensitive to high-frequency, low-amplitude variations. For high-frequency curvature, such as sinusoidal or spiraling vessels, the sum of angles metric (SOAM) is more appropriate for measuring such tortuosity (Bullitt et al. 2005a), since low-amplitude, high-frequency tortuosity does not greatly increase the total length of the vessel (which would increase the DM), but contains areas of high local curvature, elevating the SOAM. The SOAM is the integral of curvature along the vessel skeleton, normalized by the path length, where the curvature is computed by summing the angle between successive triplets of points on the centerline of a segmented vessel.

The distance metric and sum of angles metric of segmented vessels from tumors and controls were compared using a two-sided t-test in R. Tumors were also classified into 3 size categories to establish vessel populations indicative of tortuosity distributions at different stages of tumor growth, using pooled vessel sets. In addition to the categorical size classification, the tortuosity of each tumor can be summarized using the mean tortuosity metric and plotting maximum tumor diameter versus tortuosity. Linear regression by the least-squares method was used to fit a line relating tumor size to the DM and the SOAM.

In addition to these morphological descriptions of angiogenesis-induced vascular alterations, vascular density is evident in the acoustic angiography images as bright enhancement in the tumor region due to an abundance of visible vessels as well as signal detected from microbubbles in sub-resolution vasculature (see Figure 2). Since acoustic angiography is highly effective at eliminating tissue signals and detecting signals from microbubble contrast agents, intensity thresholding can be used to calculate number of voxels containing contrast in a region of interest (ROI). The vascular density of a 3-D tumor tissue volume (volumetric vascular density, or VVD) was computed by creating a mask of the tumor region of interest (ROI) using the B-mode image, applying the ROI mask to the acoustic angiography image, and using an intensity threshold to compute the percent of voxels containing microbubble contrast agent. The VVD of each tumor was compared to the vascular density of tissue adjacent to the tumors by translating the ROI mask medially by a distance approximately equal to the diameter of the tumor. ROI masks of the “normal” tissue were maintained at a depth equal to the tumor masks to avoid any attenuation effects on image intensity, and the size and shape of the tumor ROIs were not altered in the spatial translation. Tumor and normal tissue VVD were compared in 19 tumors using a paired t-test. Five tumors were not included in the VVD analysis due to the tumor position making it difficult to place a satisfactory ROI in the normal tissue.

Results

Vessels were segmented from 24 tumor-bearing mice, with tumor ranging in size from 2.02 to 6.86 mm in their largest dimension, as well as vessels from control images of healthy mice in the same age and size range as the tumor-bearing mice. Control images were acoustic angiography images of the left and right lower abdomen in the location of the inguinal mammary pads. Tumor size was determined by measuring the length, width, and

depth of each tumor in high-frequency B-mode images and tumors were grouped into 1 of 3 size bins based on the largest dimension. The 2-3 mm tumors ranged in size from 2.02 to 2.93 mm, with an average size of 2.47 mm. These small tumors are barely palpable to trained handlers, but visible with high frequency B-mode ultrasound. Tumors classified as 3-4 mm ranged from 3.01 to 3.94 mm with an average size of 3.52 mm. Tumors larger than 4 mm were grouped together and ranged from 4.13 to 6.86 mm with a mean of 5.07 mm in the maximum dimension. The total number of vessels segmented and analyzed was 2302, with 1556 of these vessels coming from control images. The number of vessels analyzed for each tumor size range increased with tumor size, resulting in an average of 21.0, 32.6, and 38.3 vessels extracted for each 2-3 mm, 3-4 mm, and >4 mm tumor image, respectively.

Both metrics of tortuosity (DM and SOAM) and the VVD, were significantly higher for the pooled tumor vessels than for the control vessels (see Figure 3). Nearly all of the tumors exhibited enhancement over the normal tissue, with the mean difference of 24.6 between the normal and tumor tissue VVD. Using a paired t-test, the difference between VVD in the tumor ($\mu = 43.8 \pm 21.5$) and surrounding tissue ($\mu = 19.5 \pm 18.0$) is significant, with $p<0.01$. The mean and standard deviation DM of the control vessels was 1.255 ± 0.371, whereas the combined tumor groups showed an elevated DM ($p<0.01$) with a mean and standard deviation of 1.431 ± 0.596, representing an increase in the mean of approximately 14%. The control vessels have a mean SOAM of 22.51 ± 9.45, while the SOAM of the combined tumor groups is increased roughly 60% from the control condition ($p<0.01$), with a mean of 35.92 ± 13.49.

Additionally, comparing the DM and SOAM between control vessels and the vessels from each of the size classifications (2-3 mm, 3-4 mm, and >4 mm) using a two-sided T-test, there is a significant difference between the control group using a cutoff of $p< 0.0167$ to represent a significance level of $\alpha=0.05$ with a Bonferroni correction to account for multiple hypothesis testing. Table 1 shows summary statistics of each size group and control vessels, including the median, mean, and standard deviation for both tortuosity metrics, as well as number of vessels analyzed and tumor size ranges. Tukey boxplots (Figure 4), in which the box defines the interquartile range (IQR) and the median, and the whiskers are located at the points 1.5 times the IQR, of the DM and SOAM show the trend of tortuosity increasing with tumor size, and reaching a plateau for tumors larger than 4 mm. This trend is also visible in Figure 5, by plotting the mean tortuosity metric of each of the 24 tumors versus size. Linear least-squares regression analysis shows positive correlation for both the DM ($R^2=0.26$) and SOAM ($R^2=0.07$), but only the trend relating tumor diameter to the distance metric is statistically significant ($p<0.01$).

Discussion

Acoustic angiography represents a substantial advance in ultrasound imaging technology and allows for meaningful quantification of vascular structure for evaluation of disease involving vascular dysfunction, especially cancer, as presented here. This method uses a standard FDA approved contrast agent (albeit off-label currently), and a new type of ultrasound imaging transducer designed to have a bandwidth much broader than existing single-frequency transducers. The acoustic pressure and frequency required for this

technique is within FDA limits as well as within the mechanical index recommendation of 0.8 for the clinical use of Definity® (Lantheus Medical Imaging, N. Billerica, MA). Although the mechanical index (MI) used in this study is above the “low MI” scheme frequently used for contrast imaging (Kim et al. 2008), higher pressures are required to produce optimal contrast to tissue ratios in acoustic angiography (Gessner et al. 2010; Lindsey et al. 2014). However, contrast imaging techniques with mechanical indices greater than used here, such as flash-replenishment, have been used safely in clinical practice for several years (Aggeli et al. 2008; Dolan et al. 2009).

We have shown that two metrics of tortuosity, the distance metric and sum of angles metric, are both increased in tumors at least 2mm in their largest dimension. The DM best describes low-frequency deviations from straight, such as vessels that grow in arching curves, whereas the SOAM accurately quantifies tortuosity of high frequency variations that represent locations of high local curvature, without greatly increasing the total length of a vessel. Both descriptions of vessel structure show an increasing trend as tumors increase in size, with the SOAM measurements showing greater magnitude changes between groups. Interestingly, the tortuosity metrics of the largest group (>4 mm tumors), which include tumors between 4 and 7 mm, seem to plateau, though variability in mean tortuosity between tumors weakens the correlations between size and tortuosity. The apparent tortuosity plateau may be due to the angiogenic signaling and neovascularization processes reaching a maximum level at this size for the tumor type studied. However, another likely explanation is that tumors over 4 mm in diameter become more noticeably heterogeneous. The variation in the location of tumor growth can cause differences in proximity to native vasculature, and thus have an influence on anisotropic patterns of angiogenesis. Additionally, these tumors tend to exhibit necrosis and/or hemorrhage as they continue to grow, and heterogeneous patterns of enhancement are visible in the acoustic angiography images as the tumors become larger. This heterogeneity in growth and vascularization is likely to also produce heterogeneity in vessel tortuosity. Both the DM and SOAM data from acoustic angiography images indicated abnormally high tortuosity at all stages of tumor evolution studied here, therefore we can hypothesize that these morphological differences are due to malignant angiogenesis, not a wound healing response from tumor initiation or other potential artifacts of a xenograft model that could contribute to angiogenesis in implanted tumor models.

Since tumor angiogenesis is common to nearly all tumor types and across species, the quantification of vascular abnormalities provides a powerful tool for studying cancer. The vessel structures visible in acoustic angiography images, and the tortuosity metrics derived therefrom, provide a clear distinction of small tumors from controls and are also sensitive to the evolution of vascular morphology that occurs during tumor growth in a pre-clinical model. Thus, the ability to directly image these blood vessels in humans would provide a powerful clinical tool for detecting early malignant lesions, evaluate early tumor treatment response, or possibly define tumor margins. Traditional clinical imaging modalities are unable to directly image the newly formed blood vessels at the necessary resolutions. Contrast enhanced computed tomography (CT) can demonstrate abnormal tissue enhancement, but is incapable of directly visualizing the vessels. Higher resolution CT techniques could be performed, but only at excessive radiation doses only appropriate for

specimens. Ultrasound power Doppler can also be performed to obtain perfusion type information, but clear microvascular structure is not visible.

Thus, we anticipate that acoustic angiography, which can directly image the tumor vessels with high resolution and contrast, can be used in adjunct to conventional imaging. The design of new transducers for human imaging will include the selection of new transmit and receive frequencies to achieve deeper, more clinically relevant imaging depths, at the expense of resolution, a topic recently explored by our group (Lindsey et al. 2014). For example, one potential application is to increase the specificity of breast ultrasound. Breast ultrasound is well known to be sensitive, but not specific in the evaluation of breast lesions, even with the use of advanced tools. However, by performing acoustic angiography during the same imaging session, one could theoretically evaluate if a lesion is a malignant or benign by visualizing the microvascular architecture within and surrounding the lesion. This approach could potentially improve our ability to characterize indeterminate lesions.

Another potential application is in the early evaluation of neoadjuvant therapy response. Early detection of tumor treatment response to chemotherapy is an important diagnostic question that could reduce inefficiencies of non-therapeutic or resistant therapies. MRI based approaches have been proposed, but are significantly more costly than ultrasound based techniques. Conventional ultrasound is primarily used to evaluate lesion size, but offers little information on the physiological status of the tumor. In this regard, acoustic angiography could potentially offer a low cost bedside support to serially evaluate tumor physiology and response to treatment.

One notable finding was that even the smallest tumors imaged in this work (2-3 mm in their largest dimension) had substantially higher tortuosity than control tissue, with statistical significance of $p<0.01$ for both the distance metric and sum of angles metric. This data suggests that it may be possible to detect sub-palpable tumors with acoustic angiography. Data also illustrates increasing measurements of microvascular tortuosity with increasing tumor size, indicating angiogenic abnormalities correlate with tumor progression. It is notable that acoustic angiography cannot directly visualize angiogenesis at the capillary scale, as vessels on the tens of microns scale are not resolvable with this technique (using the 30 MHz receiver configuration). However, vessel remodeling due to tumor angiogenesis has been observed in vasculature through a wide range of scales (Li et al. 2000; Jain 2003; Bullitt et al. 2004; Bullitt et al. 2007; Ungersma et al. 2010). Intravital microscopy imaging has demonstrated vessels close to 100 microns in diameter rapidly becoming tortuous upon injection of only 10s of tumor cells (Li et al. 2000). Although, the structure of early, small-scale angiogenic processes such as sprouting angiogenesis is not resolvable with this technique, acoustic angiography images reinforce the observation that tortuous vessel growth and remodeling occurs at multiple scales, including many vessels at least 100-200 microns in diameter that are resolvable during different stages of tumor evolution using acoustic angiography. Figure 6 shows serial imaging of tumors between 2.3 and 5.6 mm from two representative animals. Since both tortuosity metrics showed significant variation between animals, it is likely that clinical applications of acoustic angiography will include serial imaging to evaluate tortuosity changes during or after treatment, as has been done previously with MRI angiography in glioblastoma (Bullitt et al. 2009).

Major limitations of acoustic angiography include the limited depth of penetration, <2 cm in depth with the configuration here (although increased depth should be achievable with reduced resolution), and limited field of view. Field of view is limited to a small volume compared to CT or MRI, typically several cubic centimeters, as defined by the transducer configuration. Brain imaging or imaging near significant bone or gas interfaces is not possible to strong acoustic reflections which clutter the signal. Acoustic angiography also requires 3-D imaging to enable effective microvascular analysis. We currently reconstruct 3-D volumes using a transducer mechanically scanned in the elevational axis, which increases time of the imaging scan and makes the imaging technique susceptible to tissue motion, although future 2-D matrix arrays could make volumetric acoustic angiography real-time. Frame rate is also limited using the current prototypes, because the dual single-element transducer design must swing across the tissue to acquire a B-mode image. Acoustic angiography is a contrast ultrasound technique, and despite a large body of safety data (Wei et al. 2008; Dolan et al. 2009; Fine et al. 2014), contrast agents still have limited regulatory agency approval, with most applications outside of cardiology being off-label. Finally, the dual-frequency broadband transducers required for high-resolution, high signal-to-noise acoustic angiography still only exist as a handful of prototypes. However, fabrication of newer dual-frequency array devices and clinical studies of acoustic angiography in patients are underway, and will provide more information as to the ultimate clinical utility of this technique in the near future.

Conclusions

The data presented here is the first application of acoustic angiography in small (2-7 mm) tumors, and the spontaneous, autochthonous mammary tumors in the C3(1)/Tag mice imaged in this study may provide a more relevant model of cancer angiogenesis than xenograft implants since tumorogenesis occurs due to tumor suppressor gene inactivation instead of implantation of foreign tissue (typically on the order of 10^6 cells). Enhancement in acoustic angiography images was quantified as volumetric vascular density, which was shown to be significantly elevated in tumor tissue compared to control tissue adjacent to tumors. Additionally, two quantifications of vessel morphology, the distance metric and sum of angles metric show increased tortuosity for small 2-3 mm tumors, relative to control animals and these metrics tend to increase with tumor size, eventually reaching a plateau. The unique information gained from dual-frequency, acoustic angiography provides an exciting new tool for studying tumor growth and angiogenesis in pre-clinical models, and may eventually benefit clinical patients with pathologies involving vascular dysfunction.

Acknowledgements

This research was supported by National Institutes of Health 1R01CA170665 and 1R43CA165621, as well as training grant T32HL069768. We thank the directors and personnel of the UNC Lineberger Comprehensive Cancer Center's (LCCC) Mouse Phase One Unit (MP1U), especially David Darr, for their assistance. Work in the MP1U was supported by the University Cancer Research Fund. Animal Studies were performed with the assistance of the LCCC Animal Studies Core at the University of North Carolina at Chapel Hill. The LCCC Animal Studies Core is supported in part by an NCI Center Core Support Grant (CA16086) to the UNC LCCC. We also thank Juan Rojas, Sneha Rao, and Sandeep Kasoji, for assistance with data acquisition and analysis, James Tsuruta for contrast agent formulation, Marc Lukacs for prototype transducer design and fabrication, and Elizabeth Bullitt for vessel analysis algorithms.

References

Aggeli C, Giannopoulos G, Roussakis G, Christoforatou E, Marinos G, Toli C, Pitsavos C, Stefanadis C. Safety of myocardial flash-contrast echocardiography in combination with dobutamine stress testing for the detection of ischaemia in 5250 studies. Heart. 2008; 94:1571–7. [PubMed: 18474538]

Averkiou M, Powers J, Skyba D, Bruce M, Jensen S. Ultrasound contrast imaging research. Ultrasound Quarterly. 2003; 19:27–37. [PubMed: 12970614]

Aylward SR, Bullitt E. Initialization, noise, singularities, and scale in height ridge traversal for tubular object centerline extraction. IEEE transactions on medical imaging. 2002; 21:61–75. [PubMed: 11929106]

Badea CT, Drangova M, Holdsworth DW, Johnson GA. In vivo small-animal imaging using micro-CT and digital subtraction angiography. Physics in medicine and biology. 2008; 53:R319–50. [PubMed: 18758005]

Bullitt E, Ewend M, Vredenburgh J, Friedman A, Lin W, Wilber K, Zeng D, Aylward SR, Reardon D. Computerized assessment of vessel morphological changes during treatment of glioblastoma multiforme: report of a case imaged serially by MRA over four years. Neuroimage. 2009; 47(Suppl 2):T143–51. [PubMed: 19103295]

Bullitt E, Ewend MG, Aylward S, Lin W, Gerig G, Joshi S, Jung I, Muller K, Smith JK. Abnormal vessel tortuosity as a marker of treatment response of malignant gliomas: preliminary report. Technol Cancer Res Treat. 2004; 3:577–84. [PubMed: 15560715]

Bullitt E, Gerig G, Pizer SM, Lin W, Aylward SR. Measuring tortuosity of the intracerebral vasculature from MRA images. IEEE transactions on medical imaging. 2003; 22:1163–71. [PubMed: 12956271]

Bullitt E, Muller KE, Jung I, Lin W, Aylward S. Analyzing attributes of vessel populations. Medical image analysis. 2005a; 9:39–49. [PubMed: 15581811]

Bullitt E, Reardon DA, Smith JK. A Review of Micro and Macro Vascular Analyses in the Assessment of Tumor-Associated Vasculature as Visualized by MR. Neuroimage. 2007; 37:S116–S9. [PubMed: 17512217]

Bullitt E, Wolthusen PA, Brubaker L, Lin W, Zeng D, Van Dyke T. Malignancy-associated vessel tortuosity: a computer-assisted, MR angiographic study of choroid plexus carcinoma in genetically engineered mice. AJNR American journal of neuroradiology. 2006; 27:612–9. [PubMed: 16552004]

Bullitt E, Zeng D, Gerig G, Aylward S, Joshi S, Smith JK, Lin W, Ewend MG. Vessel tortuosity and brain tumor malignancy: a blinded study. Academic radiology. 2005b; 12:1232–40. [PubMed: 16179200]

Carmeliet P, Jain RK. Molecular mechanisms and clinical applications of angiogenesis. Nature. 2011; 473:298–307. [PubMed: 21593862]

Chang YC, Huang YH, Huang CS, Chang RF. Vascular morphology and tortuosity analysis of breast tumor inside and outside contour by 3-D power Doppler ultrasound. Ultrasound in medicine & biology. 2012; 38:1859–69. [PubMed: 22975041]

Dolan MS, Gala SS, Dodla S, Abdelmoneim SS, Xie F, Cloutier D, Bierig M, Mulvagh SL, Porter TR, Labovitz AJ. Safety and efficacy of commercially available ultrasound contrast agents for rest and stress echocardiography a multicenter experience. Journal of the American College of Cardiology. 2009; 53:32–8. [PubMed: 19118722]

Duncan J, Whittle M, Nakamura K, Abell A, Midland A, Zawistowski J, Johnson N. Dynamic Reprogramming of the Kinome in Response to Targeted MEK Inhibition in Triple-Negative Breast Cancer. Cell. 2012; 149:307–21. [PubMed: 22500798]

Feig SA, Shaber GS, Patchefsky A, Schwartz GF, Edeiken J, Libshitz HI, Nerlinger R, Curley RF, Wallace JD. Analysis of clinically occult and mammographically occult breast tumors. AJR American journal of roentgenology. 1977; 128:403–8. [PubMed: 190908]

Feingold S, Gessner R, Guracar IM, Dayton PA. Quantitative volumetric perfusion mapping of the microvasculature using contrast ultrasound. Investigative radiology. 2010; 45:669–74. [PubMed: 20808232]

Fine NM, Abdelmoneim SS, Dichak A, Kushwaha SS, Park SJ, Mulvagh SL. Safety and feasibility of contrast echocardiography for LVAD evaluation. JACC Cardiovascular imaging. 2014; 7:429–30. [PubMed: 24742894]

Folkman J. Tumor Angiogenesis: Therapeutic Implications. New England Journal of Medicine. 1971; 285:1182–6. [PubMed: 4938153]

Gessner R, Lukacs M, Lee M, Cherin E, Foster FS, Dayton PA. High-resolution, high-contrast ultrasound imaging using a prototype dual-frequency transducer: in vitro and in vivo studies. IEEE transactions on ultrasonics, ferroelectrics, and frequency control. 2010; 57:1772–81.

Gessner RC, Aylward SR, Dayton PA. Mapping microvasculature with acoustic angiography yields quantifiable differences between healthy and tumor-bearing tissue volumes in a rodent model. Radiology. 2012; 264:733–40. [PubMed: 22771882]

Gessner RC, Frederick CB, Foster FS, Dayton PA. Acoustic angiography: a new imaging modality for assessing microvasculature architecture. Int J Biomed Imaging. 2013; 2013:936593. [PubMed: 23997762]

Hanahan D, Weinberg RA. Hallmarks of cancer: the next generation. Cell. 2011; 144:646–74. [PubMed: 21376230]

Huang SF, Chang RF, Moon WK, Lee YH, Chen DR, Suri JS. Analysis of tumor vascularity using three-dimensional power Doppler ultrasound images. IEEE transactions on medical imaging. 2008; 27:320–30. [PubMed: 18334428]

Jain RK. Molecular Regulation of Vessel Maturation. Nature Medicine. 2003; 9:685–93.

Jain RK. Normalization of tumor vasculature: an emerging concept in antiangiogenic therapy. Science. 2005; 307:58–62. [PubMed: 15637262]

Jain RK. Antiangiogenesis strategies revisited: from starving tumors to alleviating hypoxia. Cancer cell. 2014; 26:605–22. [PubMed: 25517747]

Jain RK, Martin JD, Stylianopoulous T. The role of mechanical forces in tumor growth and therapy. Annu Rev Biomed Eng. 2014; 16:321–46. [PubMed: 25014786]

Kim TK, Jang HJ, Burns PN, Murphy-Lavallee J, Wilson SR. Focal nodular hyperplasia and hepatic adenoma: differentiation with low-mechanical-index contrast-enhanced sonography. AJR American journal of roentgenology. 2008; 190:58–66. [PubMed: 18094294]

Kruse DE, Ferrara KW. A new imaging strategy using wideband transient response of ultrasound contrast agents. IEEE transactions on ultrasonics, ferroelectrics, and frequency control. 2005; 52:1320–9.

Laufer J, Johnson P, Zhang E, Treeby B, Cox B, Pedley B, Beard P. In vivo preclinical photoacoustic imaging of tumor vasculature development and therapy. J Biomed Opt. 2012; 17:056016. [PubMed: 22612139]

Li CY, Shan S, Huang Q, Braun RD, Lanzen J, Hu K, Lin P, Dewhirst MW. Initial stages of tumor cell-induced angiogenesis: evaluation via skin window chambers in rodent models. Journal of the National Cancer Institute. 2000; 92:143–7. [PubMed: 10639516]

Lindsey BD, Rojas JD, Martin KH, Shelton SE, Dayton PA. Acoustic Characterization of Contrast-to-tissue Ratio and Axial Resolution for Dual-Frequency Contrast-Specific “Acoustic Angiography” Imaging. IEEE transactions on ultrasonics, ferroelectrics, and frequency control. 2014; 61:1668–85.

Martin KH, Dayton PA. Current status and prospects for microbubbles in ultrasound theranostics. Wiley interdisciplinary reviews Nanomedicine and nanobiotechnology. 2013; 5:329–45. [PubMed: 23504911]

Molinari F, Mantovani A, Deandrea M, Limone P, Garberoglio R, Suri JS. Characterization of single thyroid nodules by contrast-enhanced 3-D ultrasound. Ultrasound in medicine & biology. 2010; 36:1616–25. [PubMed: 20800947]

Molinari F, Meiburger KM, Giustetto P, Rizzitelli S, Boffa C, Castano M, Terreno E. Quantitative Assessment of Cancer Vascular Architecture by Skeletonization of High-resolution 3-D Contrast-enhanced Ultrasound Images: Role of Liposomes and Microbubbles. Technology in cancer research & treatment. 2014; 13:541–50. [PubMed: 24206210]

Nissen NN, Polverini PJ, Koch AE, Volin MV, Gamelli RL, DiPietro LA. Vascular endothelial growth factor mediates angiogenic activity during the proliferative phase of wound healing. The American journal of pathology. 1998; 152:1445–52. [PubMed: 9626049]

Quaia E. Assessment of tissue perfusion by contrast-enhanced ultrasound. European radiology. 2011; 21:604–15. [PubMed: 20927527]

Sodi A, Guarducci M, Vauthier L, Ioannidis AS, Pitz S, Abbruzzese G, Sofi F, Mecocci A, Miele A, Menchini U. Computer assisted evaluation of retinal vessels tortuosity in Fabry disease. Acta ophthalmologica. 2013; 91:113–9.

Ungersma SE, Pacheco G, Ho C, Yee SF, Ross J, van Bruggen N, Peale FV Jr. Ross S, Carano RA. Vessel imaging with viable tumor analysis for quantification of tumor angiogenesis. Magnetic resonance in medicine. 2010; 63:1637–47. [PubMed: 20512867]

Wei K, Mulvagh SL, Carson L, Davidoff R, Gabriel R, Grimm RA, Wilson S, Fane L, Herzog CA, Zoghbi WA, Taylor R, Farrar M, Chaudhry FA, Porter TR, Irani W, Lang RM. The safety of deFinity and Optison for ultrasound image enhancement: a retrospective analysis of 78,383 administered contrast doses. Journal of the American Society of Echocardiography. 2008; 21:1202–6. [PubMed: 18848430]

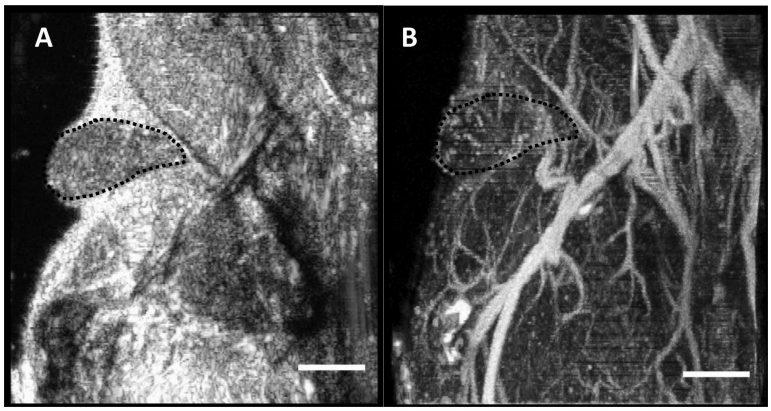

Figure 1.

Panel A shows a coronal slice reconstruction of a B-mode tissue volume. Panel B shows a maximum intensity projection of the acoustic angiography image of the same tissue volume, approximately 2.5 by 2.5 cm. The dashed outline delineates a tumor in the right inguinal mammary pad of a mouse in both images. The scale bar for both images is 4 mm.

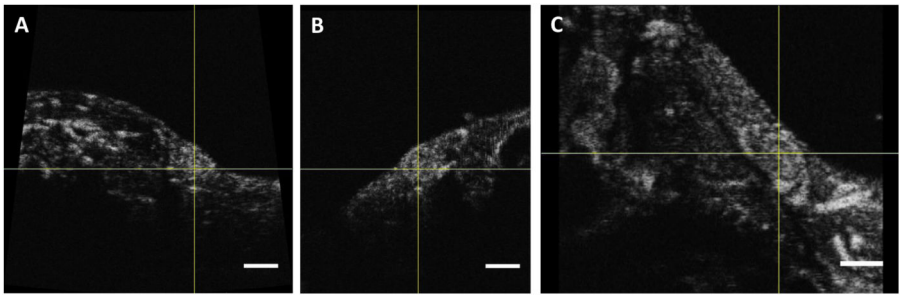

Figure 2.

Orthogonal views (single slice) of a representative tumor in acoustic angiography: Panel A shows the axial view, panel B the sagittal, and panel C the coronal (rotated 90 degrees counterclockwise). The scale bar represents 3 mm.

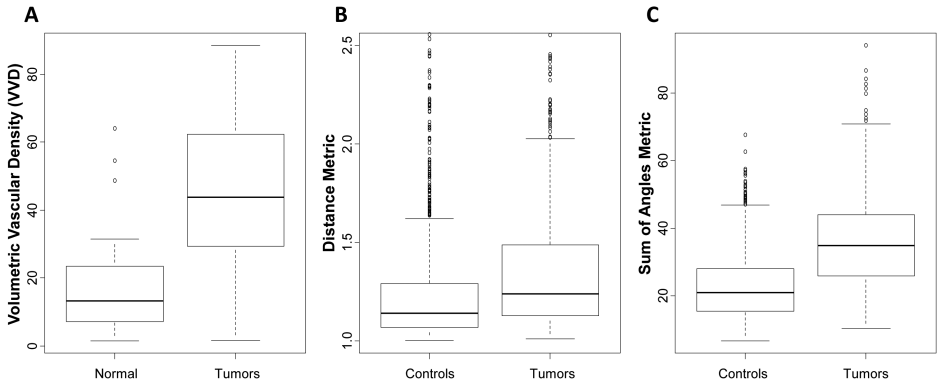

Figure 3.

Tukey boxplots comparing the volumetric vascular density (panel A), distance metric (panel B), and sum of angles metric (panel C) in tumors vs. controls. P<0.01.

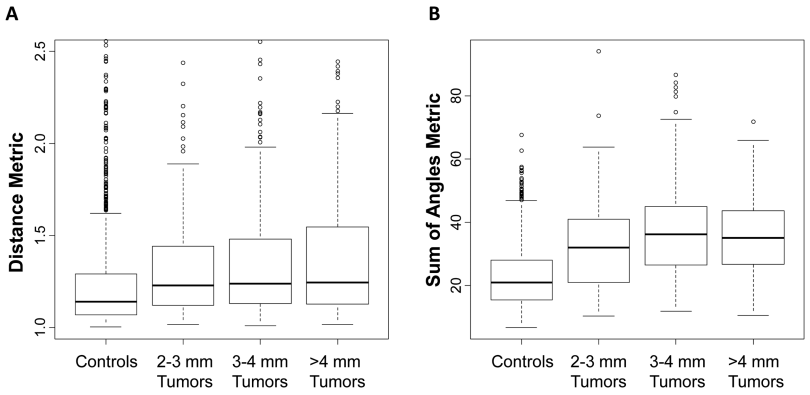

Figure 4.

Quantifications of vascular tortuosity by tumor size classification: Panel A shows Tukey boxplots of the distance metric (DM) for control vessels and 3 different sizes of tumors. Panel B shows Tukey boxplots of the corresponding sum of angles metric (SOAM) for the same sets of vessels. Each tumor group is statistically different from the control group ($p<0.0167$, Bonferroni corrected).

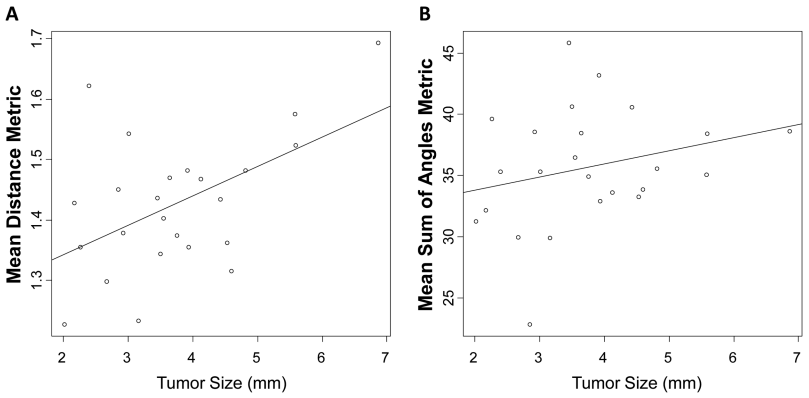

Figure 5.

Tumor size vs. the mean tortuosity metric with the least-squares regression line displayed for the 24 tumors analyzed. Panel A shows the distance metric, and panel B shows the sum of angles metric.

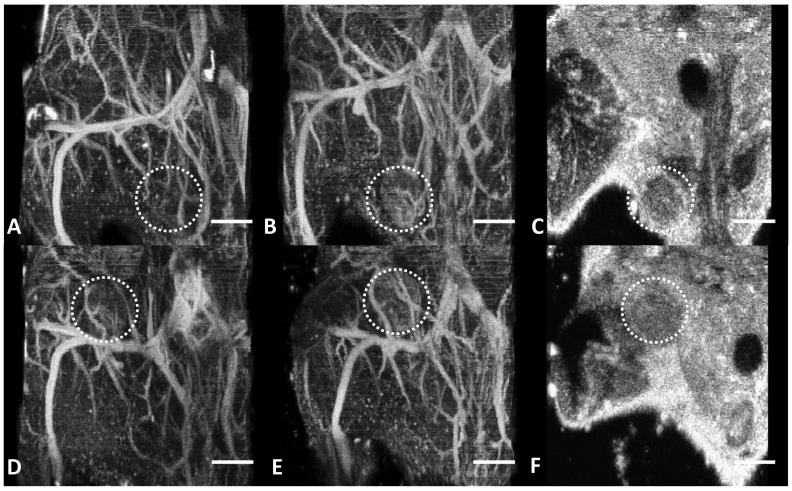

Figure 6.

Top row is animal 1: Panels A and B are acoustic angiography maximum intensity projections (MIPs) acquired 9 days apart. The tumor indicated by the dashed circle grew from 2.3 mm to 4.13 mm. Panel C shows a coronal B-mode image taken with panel B. Bottom row is animal 2: Panels D and E are acoustic angiography coronal MIPs acquired 7 days apart, and panel F is a B-mode image corresponding to panel E. The tumor circled grew from 3.8 mm to 5.6 mm. All scale bars show 4 mm, and dashed circles indicate approximate tumor locations.

Table 1

Summary Statistics for Vessel Segmentation and Tortuosity Analysis in Controls and Tumors

	Controls	2-3mm	3-4mm	>4mm
Average Tumor Size (mm)	NA	2.47	3.52	5.24
Minimum Tumor Size (mm)	NA	2.02	3.01	4.13
Maximum Tumor Size (mm)	NA	2.93	3.92	6.86
Number of Vessels	1556	147	293	306
DM-Median	1.141	1.229	1.240	1.245
DM-Mean	1.255	1.404	1.401	1.473
DM-Standard Deviation	0.371	0.576	0.514	0.672
SOAM-Median	20.91	31.92	36.17	35.14
SOAM-Mean	22.51	32.89	37.49	35.87
SOAM-Standard Deviation	9.45	14.30	14.57	11.69